MINERALOGIA POLONICA
Vol. 17, No 1—1986

Tadeusz WIESER, Witold ŻABIŃSKI**

COPPER ARSENATE AND SULPHATE MINERALS FROM MIEDZIANKA NEAR KIELCE (POLAND)

Abstract. Apart from well known and common malachite and azurite, the list of secondary minerals in the Miedzianka copper deposit (Holy Cross Mts.) includes fairly common zincian olivenite, tyrolite, brochantite and antlerite, first described by the present authors. The occurrence of staszicite, reported from this locality by Morozewicz (1919) as a new mineral, remains controversial (conichalcite according to Strunz 1939) or zincian olivenite after Guillemin (1956) and Dunin-Barkovskaya (1962). It was not confirmed by the present investigation. Zincian olivenite occurs in two varieties, less and more zinc-rich (so-called leucochalcite), easily discernible by optical and other methods. IR spectrum of Zn-olivenite is typical of the member of olivenite-adamite series with about 40% of adamite molecule. Tyrolite in spectacular specimens shows different stages of dehydration reflected, for instance, in the reduction of refractive indices and the enlargement of *d*-spacings. IR investigations of tyrolite confirmed the ordering of the structure after heating to 600°C. Both minerals are connected with Zn-bearing tennantite (miedziankite of Morozewicz, 1923) as the source copper mineral. Antlerite, less common than brochantite, precipitated from more acidic solutions as the last in the succession of copper minerals derived from primary β-chalcocite. Brochantite, as well as antlerite, yields identical decomposition products in heating experiments, though at slightly different temperatures as might be deduced from DTA analyses.

INTRODUCTION

Geological setting

Copper mineralization phenomena in Miedzianka deposit are specially related to Middle Devonian limestones, forming veiny or karst-type and "contact"-type accumulations (on erosional surfaces). These limestones are overlain by barren Rothliegendes formation. Moreover, posthumous tectonic deformations, postulated as the heritage of the Hercynian movements (Czarnocki 1929, Rubinowski 1955), were of essential importance for the migration and deposition of ore-bearing solutions. Particularly convenient in this respect were the intersections of longitudinal and transversal tectonic discontinuities. The intensity of mineralization can be illustrated by the amount of high-quality ores (over 1000 tons) mined in 1915—1919. It is also worth mentioning that the Miedzianka deposit was already mined in prehistoric times.

* Geological Institute, Carpathian Division, Cracow (31-560 Kraków, ul. Skrzatów 1).
** Academy of Mining and Metallurgy, Institute of Geology and Mineral Deposits, Cracow (30-059 Kraków, al. Mickiewicza 30).

The material to be studied was almost entirely derived from the karst-type ore deposits. These deposits are characterized by the predominance of β-chalcocite among primary copper minerals, while in vein-type deposits chalcopyrite is a prevalent mineral (Rubinowski 1955, 1971; Wojciechowski 1958). Tennantite occurs in both kinds of ore accumulations, but judging from numerous zincian olivenite and tyrolite occurrences in the karst-type deposits, tennantite seems to be typical of the latter type of mineralization.

A great number of samples collected from waste dump revealed that β-chalcocite and tennantite are preserved among the final products of carbonatization and hydration, usually in the form of malachite with or without azurite. The latter mineral forms preferentially from tennantite as a source mineral. Due to scarce and dispersed remains of primary minerals, the transformed ores show dark grey colour with green and, exceptionally, blue tint. Specific gravity determinations allow a quick evaluation of the stage of alteration. These observations point to a highly developed oxidation zone in the discussed deposit, its presence being due to variable air/water interface level.

Mode of occurrence and parageneses

Arsenate and sulphate copper minerals of the Miedzianka deposit normally occur separately depending on the nature of the primary minerals, i.e. tennantite or chalcocite. The lack of pharmacolite and other iron arsenates excludes chalcopyrite as the source mineral in this association.

Zincian olivenite is a tennantite-derived secondary mineral, forming always earlier than tyrolite. Its formation is preceded only by metasomatic transformation of tennantite into malachite and/or azurite. This sulphoarsenide is still locally preserved in small relict inclusions. Though both basic copper carbonates may also form by replacement of calcium carbonate minerals, no such case was observed in the material discussed.

Zincian olivenite was observed in three forms of occurrence, or generations, viz.: 1° — in dense, frequently veinlet-like aggregations, replacing malachitized and/or azuritized tennantite; 2° — in cavernous, vesicular masses, composed of nearly isometric, microcrystalline (up to 0.1 mm in diameter) grains (Phot. 1); and 3° — in reniform, botryoidal to stalactitic aggregates with parallel to radial arrangement of rods to fibres (Phot. 2), attaining a length of 0.25 mm. The elongated crystals are subhedral, with elongation direction parallel to [*001*], and vertical prism {*110*} or front pinacoid {*100*} as side forms. The last generation and, to some extent, the second one indicate precipitation from concentrated solutions in free space.

Macroscopically, the first two generations are distinctive by half-adamantine to glassy lustre, clearly olive-green colour with yellow to grass-green tint. The third generation has silky lustre and is faintly greyish-green, nearly colourless. These features are responsible for the name of this variety — *leucochalcite*.

Simultaneously with the third, latest generation of zincian olivenite originated the last generation of azurite in tabular crystals or rose-shaped aggregates, as well as spherical polynodules of pitch-black, X-ray amorphous asbolane (?). The generation of malachite in reniform to spherical polynodules is distinctly the last in the succession, which may generally be summarized as follows: tennantite → malachite (I) ± azurite (I) → olivenite (I) → olivenite (II) + azurite (II) ± malachite (II) → olivenite (III) = leucochalcite + azurite (III) + asbolane → malachite (III) and/or tyrolite.

Tyrolite is usually confined to the matrix of the brecciated (collapse, solution and friction breccia) gangue material composed of limestone, secondary calcite, residual clays and iron oxyhydroxides. It fills irregular voids, especially fissures. It may also finely impregnate fragments and the matrix of the gangue. Larger cavities are occupied by hemi-spherical to spherical aggregates built of radial fibres, laths or flakes, rarely by felt-like aggregates (Phots 3—5).

Tyrolite, especially that occurring in veinlets, may be accompanied by azurite crystals and their groups covering the walls or suspended in the fibrous tyrolite mass. Sometimes the gangue breccia is predominantly composed of zincian olivenite fragments with additional goethite, clay minerals a.o., which are overgrown by an azurite crust of small spherical nodules and by tyrolite felt-like aggregates of irregular shapes.

These specimens confirm the already postulated alternation of crystallization phases, namely: olivenite (II, III) → azurite (III) → tyrolite.

Brochantite is more common than the related basic copper sulphate — antlerite, and appears normally as dusty to dense microgranular crust (Phot. 6) in association with malachite and gangue component, covering more or less malachitized β-chalcocite aggregations. It can also finely impregnate gangue breccia composed of limestone, secondary calcite and clay minerals. In voids it can develop nearly euhedral crystals, sometimes, with accompanying finer-grained antlerite.

The brochantite crystals in microscopic geodes show a tabular habit caused by the pronounced development of the basal pinacoid {*001*}, accompanied by the third-order vertical prism {*210*} as well as other poorer developed chiefly prism forms, responsible for predominantly hexagonal outlines of platelets.

The deep-green with blue tint or emerald-green colour of transparent brochantite crystals reaching up to 0.25 mm in diameter, distinguishes well this mineral from the neighbouring smaller, more flattened and subhedral antlerite scaly crystals, showing more clearly yellowish- and greyish-green colour.

The noted alternation of the basic sulphate minerals of copper depends on the pH of solutions. Their acidification, usually in the latter stages of precipitation, decides that the normal succession is as follows: malachite → brochantite → antlerite.

Antlerite is confined to brecciated gangue material, where it assumes the shape of botryoidal, dense to dusty crusts (Phot. 7), as well as transsecting veinlets of a thickness up to 1 mm. The latter mode of occurrence is characterized by an oriented (perpendicular to the walls) arrangement and a somewhat more developed growth state (crystals up to 0.09 mm in diameter) in comparison with 0.05 mm large randomly distributed antlerite individuals of crusts. Furthermore, the habit of subhedral flakes and scales in veinlets shows higher elongation ratio.

As can be deduced from the optical orientation of indicatrix, the flattening plane of flakes corresponds, as a rule, to the side pinacoid {*010*}, being simultaneously a perfect cleavage plane.

In some brochantite impregnations of gangue, antlerite concentrates in the peripheral parts, indicating its late or even hypergenetic origin. The two minerals are antagonistic in relation to the described copper arsenates due to the nature of the primary copper minerals.

LABORATORY EXAMINATIONS

Optical properties

Zincian olivenite reveals remarkable variability in optical properties, especially in optical density, owing to the changing chemical constitution. This feature is detectable even in a simple crystal, implying varying concentrations of copper and zinc during precipitation.

The distribution of zinc-rich cones of growth in the third generation (leucochalcite) rod-type crystals with a typical hourglass structure (birefringence sector zoning) is indicative of increasing zinc content in the later and faster growing (here equivalent to the {*001*} form) growth cones.

In the series of differents generations of zincian olivenite the chemical composition changes in general towards the members of olivenite-adamite solid-solution series richer in adamite molecule. This is evidenced by the decrease in refractive indices, as shown by the average values for the two earlier (I and II) and the last (III = leucochalcite) generations. Compared with the other published data, the following average values were obtained:

	generations I-II	generation III
n_γ	1.838 ± 0.002	1.815 ± 0.002
n_β	$1.797—8 \pm 0.001$	$1.778—9 \pm 0.001$
n_α	1.762 ± 0.002	$1.747—8 \pm 0.002$

The obtained values indicate a 74 and 53% content of olivenite molecule, respectively, in the examined samples.

The determination of n_β is considered to be the most reliable, owing to the stable orientation of this optical vector parallel to the elongation direction, i.e. [*001*], of fibres. The n_α and n_γ, on the other hand, can be evaluated only statistically (the lowest and highest values of n, resp.). It must be remembered that they change according to the kind and development of side form faces of fibres.

Other optical properties, such as birefringence, optic axial angle ($2V_\alpha = 88—89° \pm 1°$), strong dispersion ($r < v$), and weak pleochroism (γ — green with yellow shade, β — green with faintly blue shade, α — faintly greenish, with $\alpha < \gamma < \beta$) are less indicative and convenient for diagnostic purposes. The same applies to specific gravity, averaging 4.195 g/cm³.

Tyrolite, on the other hand, has fairly uniform optical properties, with variations presumably caused only by dehydration processes (e.g. $n_\gamma = 1.705$ after Guillemin 1956 and 1.730 after Larsen 1921), manifesting themselves in the appearance of dull lustre.

In the specimens with distinct glassy lustre and green-blue colour, the average optical features may be summarized as follows: $n_\gamma = 1.719 \pm 0.002$, $n_\beta = 1.713 \pm 0.002$, $n_\alpha = 1.685 \pm 0.001$; γ — grass-green with distinct blue tint, β — yellowish green, α — grass-green with distinct blue tint, $\gamma \geq \alpha > \beta$; $2V_\alpha = 74—75° \pm 1°$; distinct dispersion with $r > v$.

The recorded optic axial angle values, determined on flakes flattened parallel to {*010*} and somewhat elongated according to {*001*} = β, differ markedly from the usually cited data ($2V_\alpha = 36° \pm 3°$, see Palache *et al.* 1951). Measured on the special mounting using universal stage procedures, they suggest the existence of polytypic structural modifications. This conclusion is borne out by the absence of polarized light extinction.

Much more common is another habit in the form of fan-or sheaf-shaped, sectile assemblages of highly elongated laths (after {*010*}) displaying different optical orientation. Often flattened parallel to {*001*}, the plane of perfect cleavage, they allow a determination of n_γ, and more precisely n_α, an optical vector parallel to the elongation direction. The looseness of lath (fibre) aggregates makes the measured specific gravity values definitely lower (2.91 g/cm³) than the calculated one (3.27 g/cm³).

In immersion, **brochantite** crystals and their fragments usually disclose a preferred optical orientation with the obtuse bisectrix γ (Z) almost normal to the basal pinacoid {*001*}. Less commonly, the preferred orientation of crystal fragments and especially of perfect cleavage scales parallel to front pinacoid {*100*}, including α and β

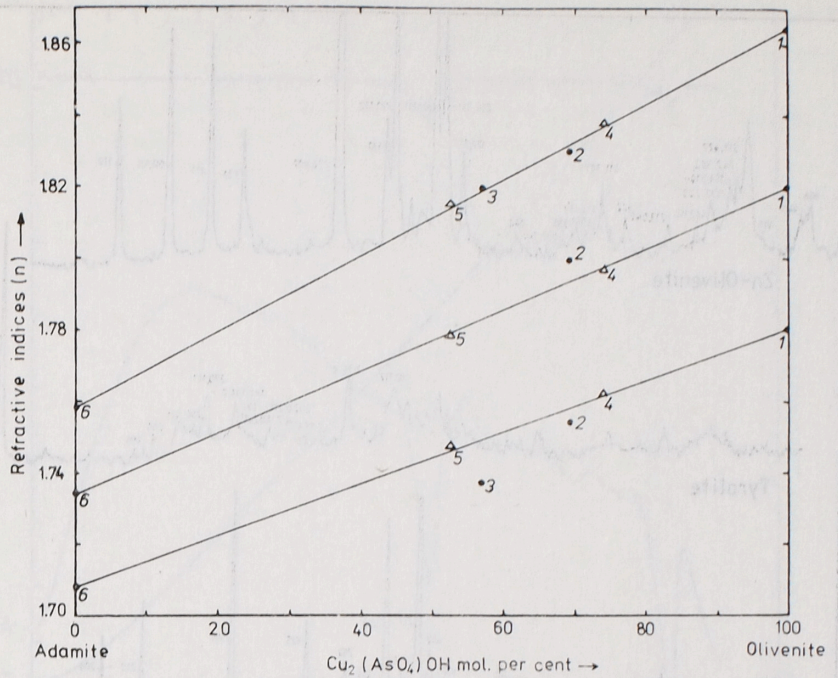

Fig. 1. Variation of refractive indices in the adamite-olivenite solid solution series *1* — olivenite from Chuquicamata, Chile (Jarrel 1939); *2, 3* — Zn-olivenites from Latchin-Khan, USSR (Dunin-Barkovskaya 1960); *4, 5* — Zn-olivenites from Miedzianka, Poland; *6* — adamite from Laurium, Greece (Larsen 1921)

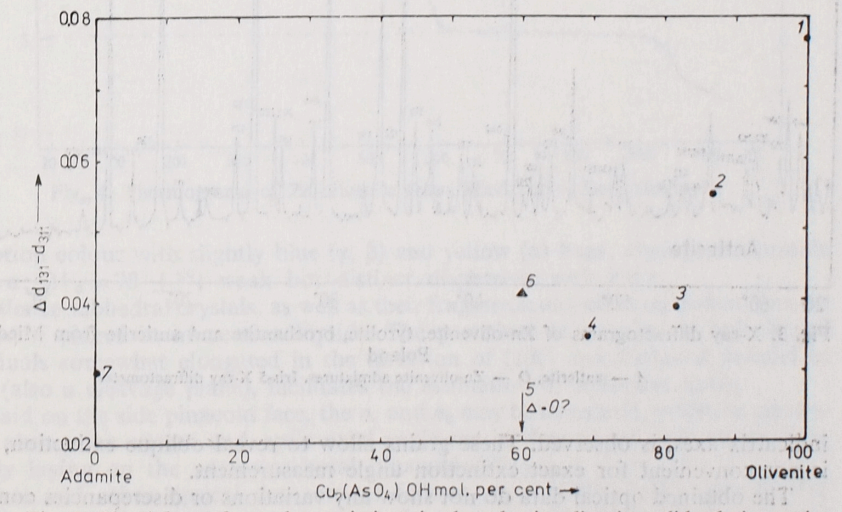

Fig. 2. The $\Delta d_{131}—d_{311}$ value variations in the adamite-olivenite solid-solution series *1* — synthetic olivenite (Minčeva-Stefanova 1964) and natural olivenite from Tintic, USA (Berry 1951); *2, 3* — synthetic Zn-olivenite (Minčeva-Stefanova 1964); *4, 5* — Zn-olivenite from Lat-chin-Khan, USSR (Dunin-Barkovskaya 1960); *6* — Zn-olivenite from Miedzianka, Poland: *7* — adamite from Mapini, Mexico (Mrose 1948)

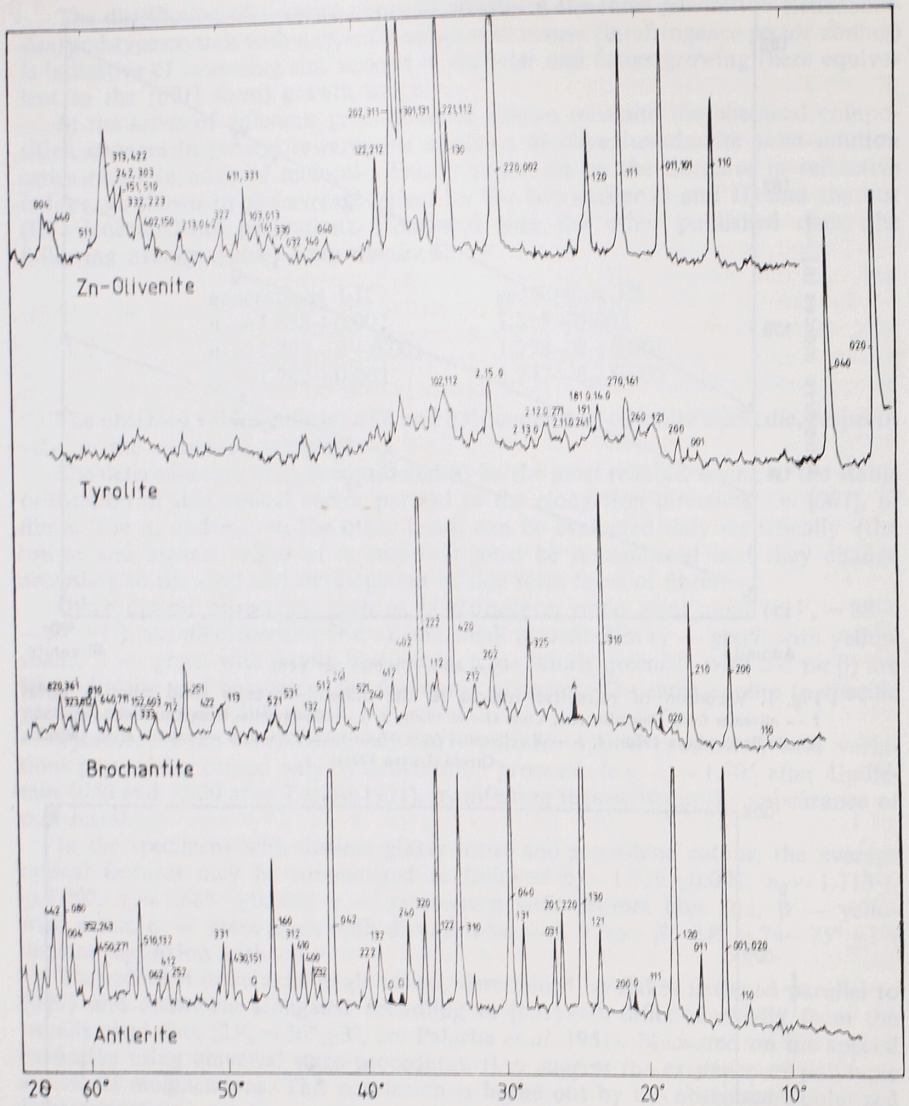

Fig. 3. X-ray diffractograms of Zn-olivenite, tyrolite, brochantite and antlerite from Miedzianka, Poland

A — antlerite, *O* — Zn-olivenite admixtures. Iris-5 X-ray diffractometer

indicatrix axes, is observed. These grains allow to reveal oblique extinction, which is not convenient for exact extinction angle measurement.

The obtained optical data do not show any variations or discrepancies compared with the published ones. In particular, worth noting is the uniformity of refractive power, testifying to the stable chemical composition of brochantite.

The refractive indices and other optical features of brochantite are: $n_\gamma = 1.799 \pm \pm 0.002$, $n_\beta = 1.770 \pm 0.002$, $n_\alpha = 1.728 \pm 0.002$; weakly pleochroic showing green

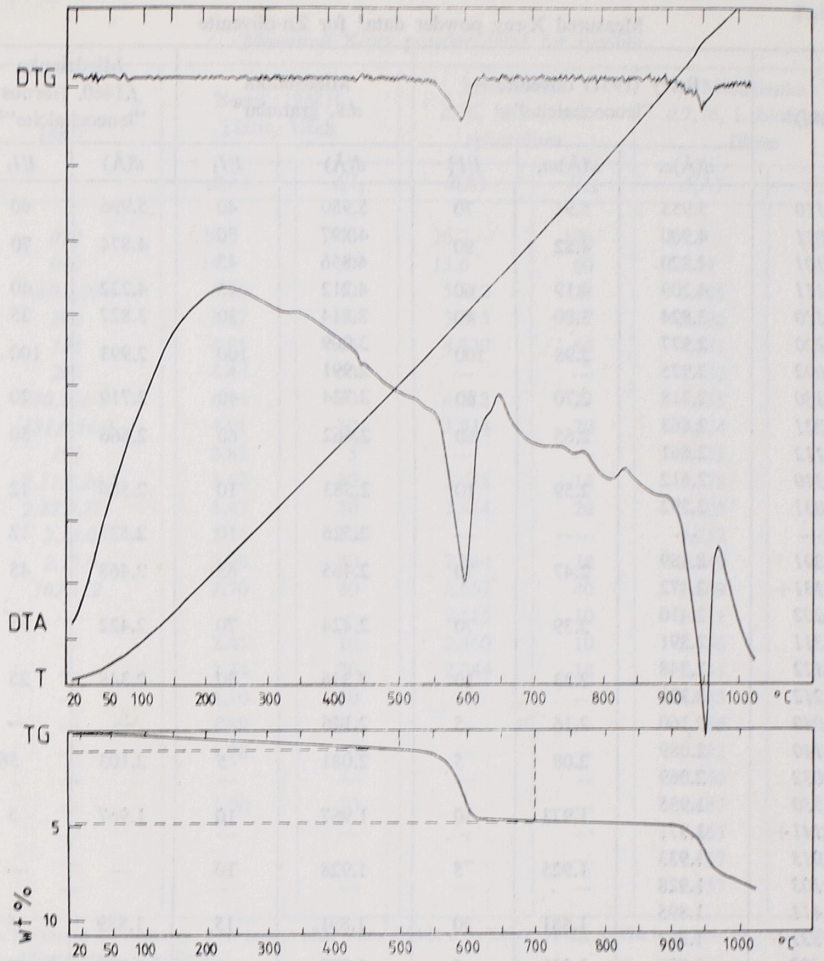

Fig. 4. Thermograms of Zn-olivenite from Miedzianka. Derivatograph

absorption colour with slightly blue (γ, β) and yellow (α) hues; absorption formula $\gamma \geqslant \beta \geqslant \alpha$; $2V_\alpha = 78° \pm 1°$; weak but distinct dispersion with $r < v$.

Antlerite subhedral crystals, as well as their fragments and cleavage flakes, become oriented if placed in immersion liquids. The prevalent orientation of lath-shaped individuals somewhat elongated in the direction of [*100*] and flattened parallel to {*010*} (also a cleavage plane), facilitates the estimation of refractive index.

If laid on the side pinacoid face, the n_γ and n_β may be measured, while the remaining n_α absorption vector and optic axial angle can be determined only on the laths scarcely laying on the narrower basal pinacoid {*001*}.

These and other optical data are as follows: $n_\gamma = 1.787 \pm 0.002$, $n_\beta = 1.737 \pm \pm 0.002$, $n_\alpha = 1.726 \pm 0.002$; γ — green, β — green with blue tint, α — pale greenish with yellow tint; $\beta > \gamma > \alpha$; $2V_\gamma = 50° \pm 1°$; very strong dispersion with $r \ll v$.

Like in brochantite, the stability of optical features in antlerite is striking, due to the stable chemical composition.

Table 1

Measured X-ray powder data[1] for Zn-olivenite

(*hkl*)[2]	Berry (1951) olivenite + "leucochalcite"			Miedzianka *d*.8, granular[4]		Miedzianka *f*.1460, fibrous "leucochalcite"[5]	
	d(Å)*c*.	*d*(Å)*m*.	I/I_1^3	*d*(Å)	I/I_1	*d*(Å)	I/I_1
110	5.955	5.91	70	5.980	40	5.996	60
011	4.900	4.82	90	4.897	50	4.874	70
101	4.820			4.856	45		
111	4.209	4.19	60	4.212	45	4.222	40
120	3.824	3.80	40	3.814	30	3.827	35
220	2.977	2.98	100	3.009	100	2.993	100
002	2.975			2.991			
130	2.718	2.70	40	2.724	40	2.719	20
221	2.663	2.65	60	2.662	60	2.666	50
112	2.661						
310	2.612	2.59	10	2.583	10	2.586	12
031	2.592						
—	—	—	—	2.526	10	2.527	12
301	2.489	2.47	70	2.465	65	2.468	45
131+	2.472						
202	2.410	2.39	70	2.424	70	2.422	55
311	2.391						
122	2.348	2.33	10	2.336	30	2.348	25
212	2.321						
040	2.160	2.16	5	2.146	5	—	—
140	2.089	2.08	5	2.081	5	2.103	56
032	2.069						
330	1.985	1.973	10	1.967	10	1.967	5
141+	1.971						
013	1.933	1.925	5	1.928	10	—	—
103	1.928						
411	1.895	1.881	20	1.891	15	1.889	5
331+	1.883						
322	1.826	1.831	5	1.838	5	1.842	10
213	1.749						
042	1.748	1.740	10	1.741	15	1.745	10
402	1.691	1.686	10	1.684	10	—	—
150	1.691						
332	1.651	1.647	20	1.656	20	1.664	10
223	1.651						
151	1.627	1.621	10	1.621	12	—	—
510	1.615						
242	1.608	1.600	30	1.596	30	1.605	12
303+	1.607						
313	1.580	1.575	60	1.587	55	1.586	35
422	1.574						
511	1.559	1.556	5	1.569	10	—	—
440	1.489	1.488	50	1.498	25	1.499	20
004	1.487			1.485	25	1.489	20

1 — Ni-filtered Cu-radiation. *2* — indices after Berry (1951). *3* — intensities as listed in ASTM card 4—657. *4* — Iris 5, Zeiss-Jena diffractometer measurement data for light olive-green olivenite in association with malachite and azurite. *5* — film measurement data (camera diameter = 114.6 mm.) for almost colourless, silky aggregates of radial-fibrous olivenite (variety called leucochalcite). *6* — additional line with 2.032 Å spacing and 5 intensity values was also observed. Abbreviations: *d*. — diffractogram, *f*. — film, *c*. — calculated, *m*. — measured.

Table 2

Measured X-ray powder data[1] for tyrolite

(*hkl*)[2]	Berry (1948)[3] Tintic, Utah		Miedzianka *d*.36, blue-green spherulites		Miedzianka *d*.7,76, l. blue-green fibres	
	d(Å)	I/I_1	*d*(Å)	I/I_1	*d*(Å)	I/I_1
020	28.0	100	26.7	100	27.1	100
040	14.1	80	13.6	60	13.57	60
0.10.0,001	5.60	30	5.512	20	5.605	15
200	5.27	40	5.215	17	5.190	18
121	4.85	60	4.730	45	4.741	35
260	4.44	50	—	—	4.480	10
270,161+	4.34	30	4.312	23	4.335	30
181,0.14.0	4.01	10	3.934	20	3.924	25
191	3.83	5	—	—	3.831	12
2.11.0,241	3.62	30	3.678	15	3.578	15
2.12.0,271	3.43	30	3.414	20	3.405	20
2.13.0	3.26	10	—	—	3.252	10
2.15.0	2.98	80	2.944	38	2.949	40
102,112	2.70	80	2.667	40	2.669	40
—	—	—	2.515	10	2.511	15
—	2.45	10	2.460	10	2.456	22
—	2.34	30	2.344	18	2.345	18
—	2.10	10	—	—	2.085	20
—	1.89	10	—	—	1.886	15
—	1.78	30	—	—	1.792	10
—	—	—	—	—	1.740	15
—	1.70	30	—	—	1.687	12
—	—	—	—	—	1.665	12
—	—	—	—	—	1.617	10
—	—	—	—	—	1.557	15

1 — Ni-filtered Cu-radiation. *2* — indices after Berry (1948). *3* — Berry (1948), ASTM card 11—348. Abbreviations: *d*. — diffractogram, *l*. — light.

X-ray data

The X-ray powder data were suitable for identification purposes, and in the case of zincian olivenite also for the determination of the chemical composition of the member of the olivenite-adamite solid-solution series.

Zincian olivenite was found, as already mentioned, in three generations. The first and second were Zn-poorer, while the third, latest generation, referred to as leucochalcite, was the richest in adamite molecule. This is well reflected by optical density (Fig. 1) but hardly so by interplanar spacings (Fig. 2). The most convenient for this purpose is the splitting of 311—202 and 131—301 reflections (Tab. 1, Fig. 3). Less suitable are 221—112 and 130 reflections preferred by Minčeva-Stefanova (1964). The mean value of Δd_{131}—d_{311} amounting to 0.041 Å indicates about 40% of adamite molecule. This observation was supported by the quantitative atomic absorption determination of Cu and Zn content in the averaged sample.

The X-ray data for other investigated minerals are in good agreement with those published by other authors (Tab. 2—4).

Table 3

Measured X-ray powder data[1] for brochantite

(*hkl*)[2]	de Wolff (1955)[3] synthetic material		Sapountzis (1972), Greece natural material		Miedzianka *f*.1541, dense coatings[4]		Miedzianka *f*.1535, dusty coatings[5]	
	d(Å)	I/I_1	*d*(Å)	I/I_1	*d*(Å)	I/I_1	*d*(Å)	I/I_1
110	7.80	8	7.80	8	7.795	15	7.839	5
200	6.38	40	6.39	53	6.403	65	6.395	65
210	5.36	40	5.37	45	5.372	60	5.369	55
020	4.93	6	—	—	4.928	12	4.940	15
310	3.90	85	3.90	87	3.906	85	3.910	75
325	3.19	40	3.20	50	3.195	25	3.197	35
$20\bar{2}$	2.923	20	2.930	25	2.922	20	2.929	15
$21\bar{2}$	2.813	4	2.810	12	2.812	8	—	—
420	2.678	50	2.677	65	2.682	70	2.675	60
112	2.601	18	2.607	20	2.604	18	2.599	20
$22\bar{2}$	2.521	100	2.524	100	2.521	100	2.524	100
$40\bar{2}$	2.466	10	2.469	12	2.463	28	2.470[6]	30
$41\bar{2}$	2.386	14	2.391	15	2.386	15	2.387	18
240	2.300	8	—	—	2.298	8	—	—
$52\bar{1}$	2.266	14	2.272	14	2.268	15	2.270	18B
$24\bar{1}$	2.190	14	2.192	20	2.189	20	2.194	28
$51\bar{2}$	2.140	14	2.140	10	2.139	15	2.141	12
132	2.079	8	2.084	10	2.082	15	2.083	12
$53\bar{1}$	2.016	8	2.021	10	2.017	15	2.019	12
521	1.969	8	1.964	12	1.969	12	1.970	12
—	1.949[8]	6	—	—	1.949	8	—	—
412	—	—	1.892	8	—	—	—	—
113	—	—	1.826	10	1.825	22	1.827	20
422	—	—	1.793	10	1.793	10	1.796	12
251	—	—	1.748	32	1.742	55	1.744	35
$71\bar{2}$	—	—	1.712	10	1.712	18	1.715	12
$33\bar{3}$	—	—	1.681	12	1.676	20	1.676	15
$15\bar{2},60\bar{3}$	—	—	1.643	15	—[7]	—	—[7]	—
640,711	—	—	1.598	15	1.598	22	1.599	18
810	—	—	1.564	17	1.563	25	1.564	22
$323,81\bar{2}$	—	—	1.541	12	1.539	20	1.540	15
$820,36\bar{1}$	—	—	1.508	22	1.507	22	1.508	20

1 — camera diameter = 114.6 mm. Ni-filtered Cu-radiation. 2 — indices cited after Sapountzis's data. 3 — de Wolff (1955), ASTM card 13-398. 4 — in assaciation with olivenite and malachitized tennantite. 5 — with small admixture of malachite on malachitized chalcocite. 6 — line coincidence with malachite. 7 — line coincidence with Si standard. 8 — the last d-value tabulated in the ASTM card. Abbreviations: *f*. — film, *B* — broad line.

Thermal analysis

DTA, TG and DTG curves of Zn-olivenite, tyrolite, brochantite and antlerite were recorded with a *Derivatograph* (made in Hungary), the sample weight amounting to 0.1—0.2 g. An additional DTA curve was obtained for tyrolite on a *Mettler TA-2 thermoanalyzer*. In both cases the heating rate was 10°C/min.

On the DTA curve of **Zn-olivenite** (Fig. 4) two sharp endothermic peaks appear with the maxima at 600 and 950°C, both connected with a considerable weight loss.

Table 4

Measured X-ray powder data[1] for antlerite

(*hkl*)[2]	de Wolff (1955)[3] synthetic material		Mrose (1961) Chile, natural material		Miedzianka *f*.1479, fine impregnations		Miedzianka *f*.1542, dense coatings[4]	
	d(Å)	I/I_1	*d*(Å)	I/I_1	*d*(Å)	I/I_1	*d*(Å)	I/I_1
110	6.80	12	6.792	11	6.817	15	6.823	15
001, 020	6.01	25	6.026	35	6.005	50	6.000	30
011	5.40	25	5.405	15	5.411	35	5.392	30
120	4.86	100	4.853	100	4.860	100	4.862	100
111	4.52	9	4.515	6	4.531	12	4.518	8
200	4.13	8	4.122	11	4.124	8	4.134	10
121	3.79	16	3.788	15	3.797	15	3.781	10
130	3.60	77	3.597	71	3.602	80	3.607	75
201, 220	3.40	31	3.403	25	3.407	30	3.408	25
031	3.34	9	3.333	6	3.336	20	3.347	12
131	3.09	16	3.089	15	3.090	18	—[5]	—
040	3.00	18	3.003	21	3.001	18	3.010	25
112	2.762	12	2.763	9	2.759	12	2.764	18
310	2.683	77	2.683	71	2.684	60	2.686	75
122	2.566	85	2.567	71	2.567	70	2.569	85
320	2.503	26	2.502	21	2.504	25	2.503	35
240	2.430	14	2.428	9	2.430	20	2.442[5]	8
132	2.315	8	—	—	2.310	17	2.321	15
222	2.259	14	2.259	11	2.259	17	2.264	20
042	2.131	69	2.127	60	2.130	75	2.133	80
232	2.083	6	2.083	2	—	—	2.080	12
400	2.065	18	2.062	11	2.065	10	—	—
410	2.034	20	2.034	15	2.035	12	2.042	15
312	2.004	4*B*	2.002	6	2.001	10	2.007	12
160	1.946	9	1.945	13	1.945	25	1.952	10
430, 151	1.835	12	1.833	8	1.836	17	1.838	12
331	1.814	15	1.813	9	1.813	17	1.816	18
252	1.711	6	1.712	2	1.712	8	1.713	8
412	1.687	9	1.687	4	1.689	12	1.690	12
062	1.667	3	1.669	2	1.667	12	—	—
510, 132	1.634	16	1.634	18	1.635[6]	20	1.633[6]	15
450, 271	1.566	13	1.568	9	1.568	18	1.570	18
352, 243	1.551	15	1.551	13	1.553	22	1.555	20
004	1.511	12	1.513	6	1.513	12	1.513	12
080	1.500	9	1.499	9	1.500	20	1.497	15
442	1.481	21	1.483	18	1.482	25	1.483	25

1 — camera diameter = 114.6 mm. Ni-filtered Cu-radiation. *2* — indices after de Wolff and Mrose calculation data. *3* — de Wolff (1955), ASTM card 7—407. *4* — with small admixture of brochantite. *5* — line coincidence with brochantite. *6* — line coincidence with Si standard. Abbreviations: *f*. — film. *B* — broad line.

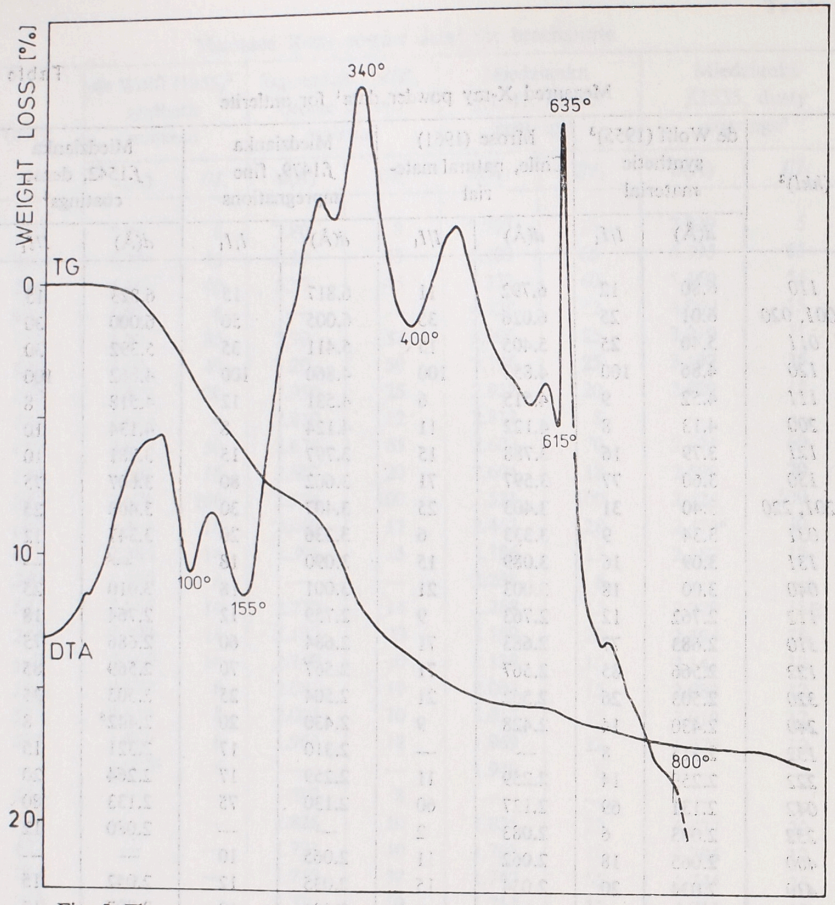

Fig. 5. Thermograms of tyrolite from Miedzianka. TA-2 Mettler thermoanalyzer

The first endothermic peak is due to dehydroxylation of olivenite. This is confirmed by an IR spectrum recorded after heating the sample for 2hrs at 700°C (Fig. 9), on which no OH absorption bands are visible. The second endothermic peak may be connected with the fusion and/or partial decomposition of the sample, as in the case of tyrolite.

The weight loss of the sample in the temperature range 20—500°C amounts to 0.7%, 500—700°C 3.9%, 700—1000°C 3.6%. The theoretical formula for olivenite points to 3.18 wt. % H_2O, the analyses of natural specimens usually showing a higher H_2O content (Dana *et al.* 1951). These data are in good agreement with the assumption that the dehydroxylation of olivenite occurs mostly in the temperature range 500—700°C.

The DTA and TG curves of **tyrolite** recorded with a Mettler microanalyzer (Fig. 5) are similar to those presented for tyrolite by Guillemin (1956). On the DTA curve at least five endothermic peaks appear in the temperature range 20—615°C, with the maxima at 100, 155, 290, 400, 560 and 615°C, followed by a sharp exothermic peak at 635°C, another exothermic peak being visible at 340°C. The TG curve

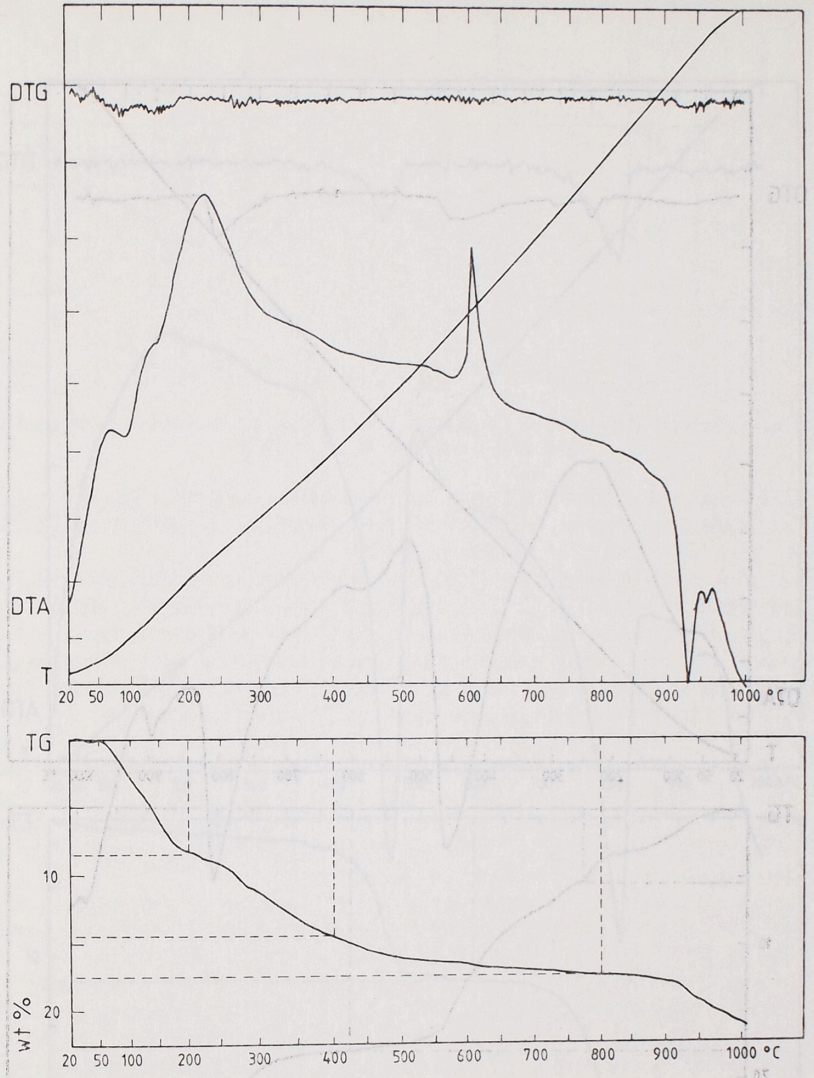

Fig. 6. Thermograms of tyrolite from Miedzianka. Derivatograph

recorded a continuous weight loss, which in the temperature range 20—200°C, corresponding to the first two endothermic effects, amounts to 8.62%, in the range 200—400°C being 6.10%, 400—600°C 2.07%, 600—800°C 1.23% (the total weight loss between 20 and 800°C is 18.02%). The bulk of molecular water is certainly lost up to 200°C. At 400°C the mineral is mostly dehydroxylated, the total water content of tyrolite (H_2O+OH) being theoretically about 18%. This is evidenced by IR absorption spectrum (Fig. 10).

On the DTA curve obtained with a Derivatograph (Fig. 6), the above endothermic effects are less pronounced. However, since this analysis was made up to a higher temperature (1000°C), a distinct sharp endothermic effect at 920°C could be seen.

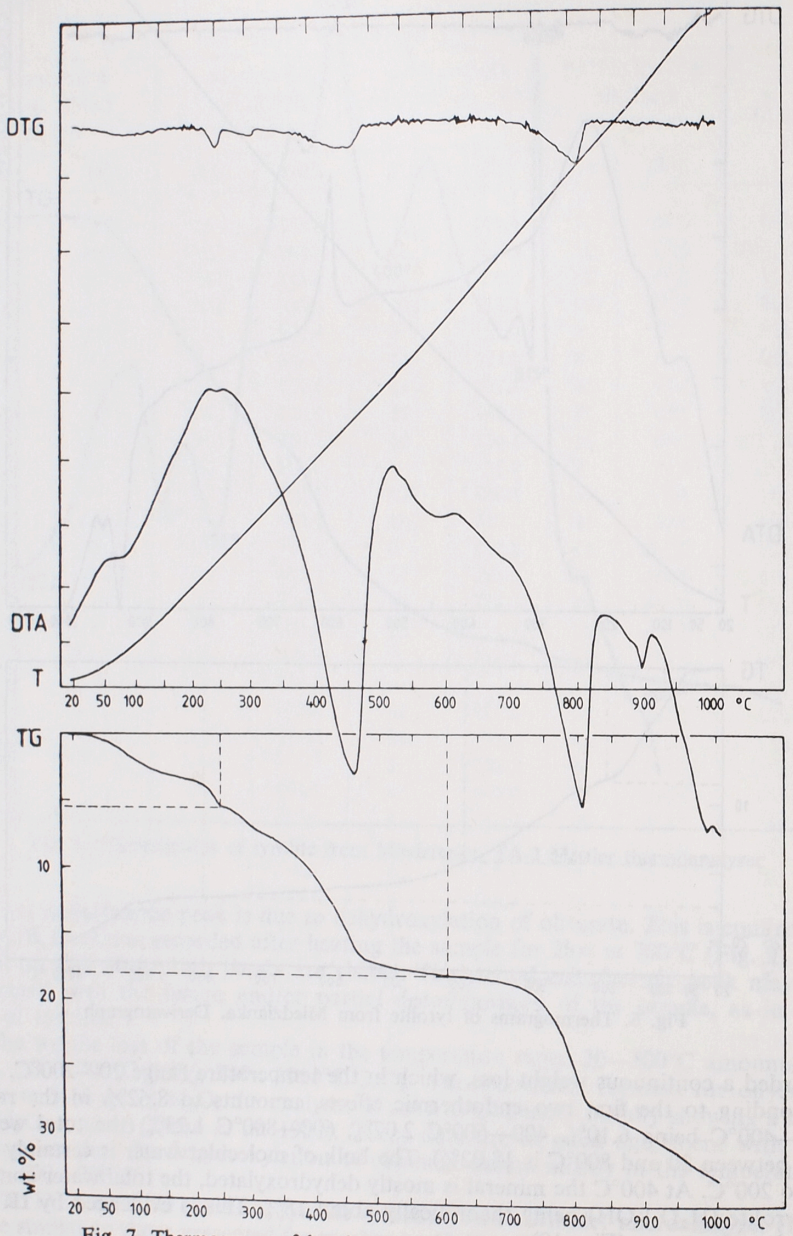

Fig. 7. Thermograms of brochantite from Miedzianka. Derivatograph

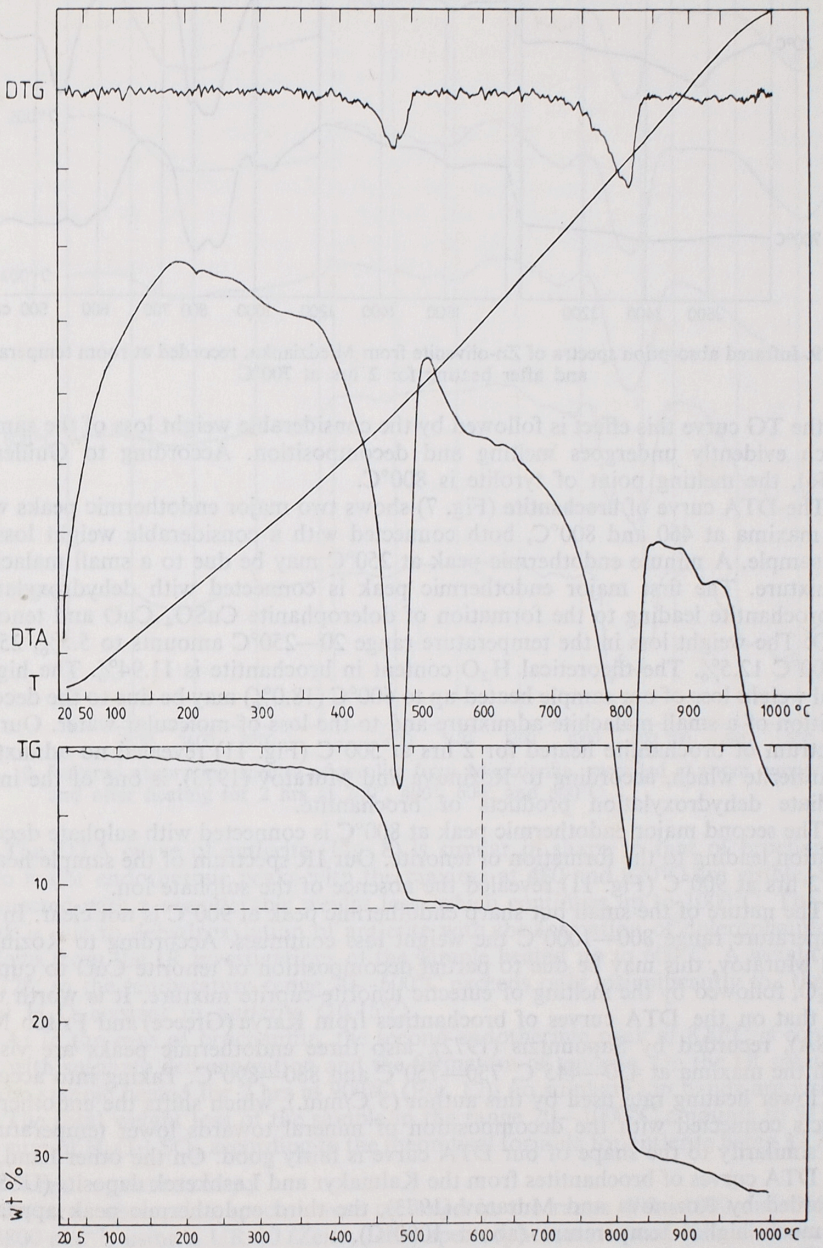

Fig. 8. Thermograms of antlerite from Miedzianka. Derivatograph

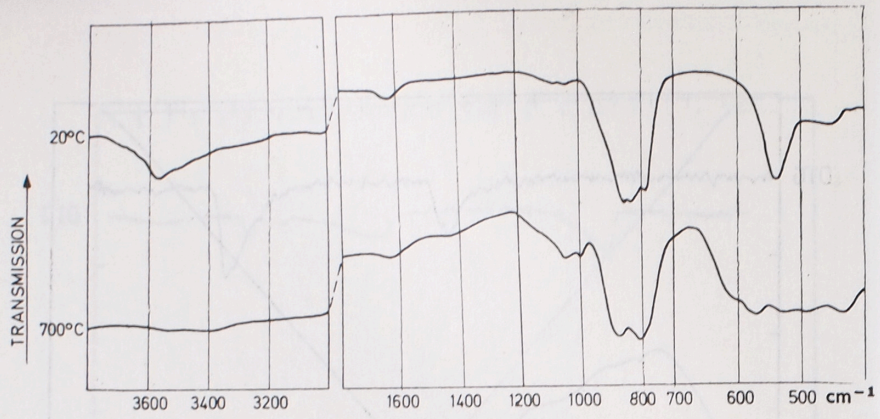

Fig. 9. Infrared absorption spectra of Zn-olivenite from Miedzianka, recorded at room temperature and after heating for 2 hrs at 700°C

On the TG curve this effect is followed by the considerable weight loss of the sample which evidently undergoes melting and decomposition. According to Guillemin (1956), the melting point of tyrolite is 800°C.

The DTA curve of **brochantite** (Fig. 7) shows two major endothermic peaks with the maxima at 460 and 800°C, both connected with a considerable weight loss of the sample. A minute endothermic peak at 250°C may be due to a small malachite admixture. The first major endothermic peak is connected with dehydroxylation of brochantite leading to the formation of dolerophanite $CuSO_4.CuO$ and tenorite CuO. The weight loss in the temperature range 20—250°C amounts to 5.5%, 250—600°C 12.5%. The theoretical H_2O content in brochantite is 11.94%. The higher total weight loss of our sample heated up to 600°C (18.0%) may be due to the decomposition of a small malachite admixture and to the loss of molecular water. Our IR spectrum of brochantite heated for 2 hrs at 500°C (Fig. 11) revealed no admixture of antlerite which, according to Rozinova and Muratov (1973), is one of the intermediate dehydroxylation products of brochantite.

The second major endothermic peak at 800°C is connected with sulphate decomposition leading to the formation of tenorite. Our IR spectrum of the sample heated for 2 hrs at 900°C (Fig. 11) revealed the absence of the sulphate ion.

The nature of the small but sharp endothermic peak at 900°C is not clear. In the temperature range 800—1000°C the weight loss continues. According to Rozinova and Muratov, this may be due to partial decomposition of tenorite CuO to cuprite Cu_2O, followed by the melting of eutectic tenorite-cuprite mixture. It is worth noting that on the DTA curves of brochantites from Karya (Greece) and Frisco Mts. (USA), recorded by Sapountzis (1972), also three endothermic peaks are visible with the maxima at 430—445°C, 730—750°C and 880—890°C. Taking into account the lower heating rate used by this author (5°C/min.), which shifts the endothermic effects connected with the decomposition of mineral towards lower temperatures, the similarity to the shape of our DTA curve is fairly good. On the other hand, on the DTA curves of brochantites from the Kalmakyr and Lashkerek deposits (USSR), recorded by Rozinova and Muratov (1973), the third endothermic peak appeared at much higher temperature (about 1080°C).

The total weight loss of our sample in the temperature range 20—1000°C amounts to 33.0%, the sum of H_2O+SO_3 according to the theoretical formula for brochantite being 29.64%.

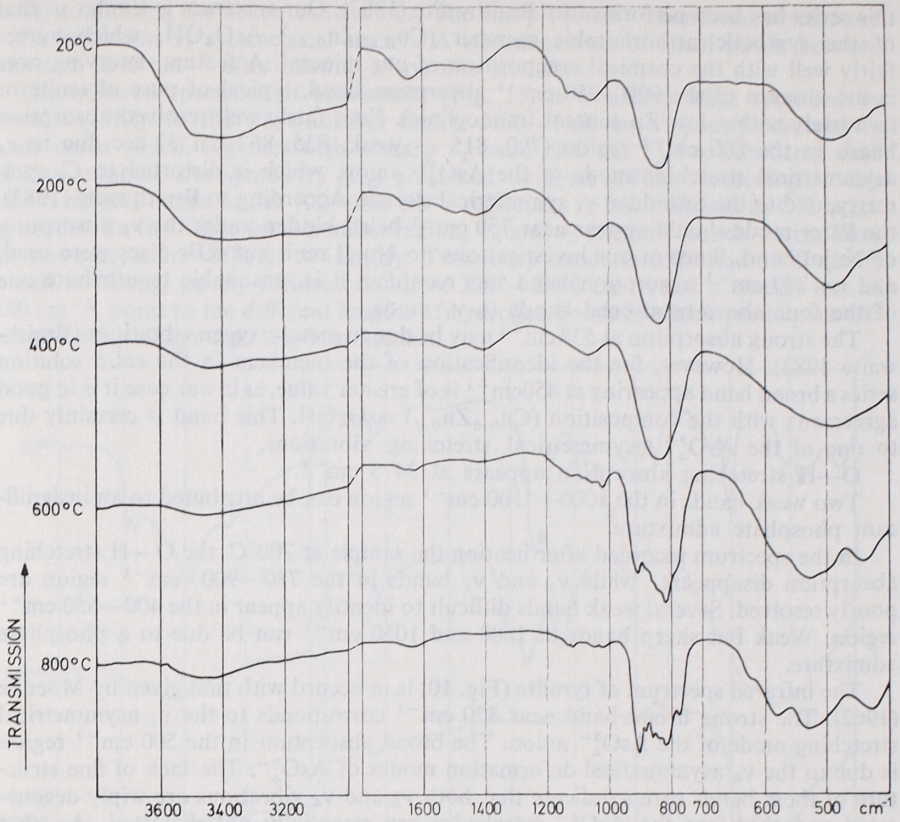

Fig. 10. Infrared absorption spectra of tyrolite from Miedzianka, recorded at room temperature and after heating for 2 hrs at 200°, 400°, 600° and 800°C

The DTA curve of **antlerite** (Fig. 8) is similar in shape to that of brochantite. Two major endothermic peaks with the maxima at 480 and 820°C are visible, both connected with a considerable weight loss, which continues up to 1000°C. The first peak is due to dehydroxylation of antlerite with the formation of dolerophanite, as follows from the IR investigations of the sample heated up to 600°C. A weight loss of 12% in the temperature range 20—600°C exceeds only insignificantly the theoretical H_2O content in antlerite (10.15%).

As in the case of brochantite, the second endothermic peak at 820°C is connected with sulphate decomposition and the formation of tenorite. On the IR spectrum of the sample heated for 2 hrs at 900°C (Fig. 12), no sulphate ion bands are visible.

The total weight loss of the sample in the range 20—1000°C amounts to 31.0%, the sum of H_2O+SO_3 according to the theoretical formula for antlerite being 32.72%.

Infrared spectroscopy

Infrared absorption spectra were recorded in the range 400—1800 and 3000—3800 cm^{-1}, using a UR-10 (Zeiss, Jena) spectrophotometer and KBr discs technique (1 mg sample + 300 mg KBr).

The infrared spectrum of olivenite (Fig. 9) is typical of an intermediate member of the solid solution series olivenite-adamite. A detailed spectroscopic analysis of

this series has been performed by Braithwaite (1983). Our spectrum is similar to that of the synthetic orthorhombic member $(Cu_{0.62}Zn_{0.38})$ AsO_4OH, which agrees fairly well with the chemical composition of our mineral. A feature deserving note is the absence of the 900—950 cm^{-1} absorption band, typical of pure olivenite or its variety with a low Zn content (monoclinic). Four fairly well resolved absorption bands in the 800 cm^{-1} region (790, 815 — weak, 835, 862 cm^{-1}) are due to ν_3 asymmetrical stretching mode of the AsO_4^{3-} anion, which is distorted to C_s symmetry, and to the forbidden ν_1 symmetrical stretch. According to Braithwaite (1983), the latter mode should appear near 750 cm^{-1} being hidden under the ν_3 absorption or Nujol band. Since in our investigations no Nujol mull but KBr discs were used, and no 750 cm^{-1} absorption band was recorded, it is reasonable to attribute one of the four above-mentioned bands to ν_1 mode.

The strong absorption at 538 cm^{-1} may be due to metal-oxygen vibrations (Braithwaite 1983). However, for the identification of the members in the solid solution series a broad band appearing at 450cm^{-1} is of greater value, as in our case it is in good agreement with the composition $(Cu_{0.6}Zn_{0.4})$ AsO_4OH. This band is certainly due to one of the AsO_4^{3-} asymmetrical stretching vibrations.

O—H stretching absorption appears at 3475 cm^{-1}.

Two weak bands in the 1000—1100 cm^{-1} region can be attributed to an insignificant phosphate admixture.

In the spectrum recorded after heating the sample at 700°C, the O—H stretching absorption disappears, while ν_3 and ν_1 bands in the 780—900 cm^{-1} region are poorly resolved. Several weak bands difficult to identify appear in the 400—650 cm^{-1} region. Weak but sharp bands at 1000 and 1050 cm^{-1} can be due to a phosphate admixture.

The infrared spectrum of **tyrolite** (Fig. 10) is in accord with that given by Moenke (1962). The strong broad band near 820 cm^{-1} corresponds to the ν_3 asymmetrical stretching mode of the AsO_4^{3-} anion. The broad absorption in the 500 cm^{-1} region is due to the ν_4 asymmetrical deformation modes of AsO_4^{3-}. The lack of fine structure of these bands seems indicate that both ν_3 and ν_4 vibrations are triply degenerated and therefore the AsO_4^{3-} tetrahedra are essentially not distorted. Another explanation could be a slight disorder of the structure and the different degree of distortion of AsO_4^{3-} tetrahedra, the broad absorptions being the result of superposition of several ν_3 as well as ν_4 bands differing in vibration frequencies. The broad band of medium intensity near 1630 cm^{-1} represents the H—O—H bending vibration of water molecules, whereas in the 3600—3300 cm^{-1} region O—H stretching absorption with the maximum at 3500 cm^{-1} is observed. O—H bending mode can be hidden under the arsenate ν_3 band (Braithwaite 1983). The nature of several weak bands in the region between 1000 and 1200 cm^{-1}, and of a weak, broad band near 1400 cm^{-1}, clearly visible also in Moenke's spectrum, is less obvious. The former might be due to a small admixture of phosphate ions.

After heating the tyrolite at 200° and 400°C, H_2O absorption disappears and OH absorption diminishes markedly. At 600°C a different spectrum appears, indicating — in accord with Guillemin's (1956) observations — the rearrangement of the structure of this mineral. In the spectrum recorded after heating the tyrolite at 800°C, this rearrangement is yet more pronounced. The splitting of the AsO_4^{3-} ν_3 band, giving at least six absorption maxima, points to the complete removal of degeneracy, and thus to the considerable distortion of the arsenate ion (Adler, Kerr 1965). Moreover, since the ν_3 band can be triply degenerated, the six maxima testify to the existence of two non-equivalent AsO_4^{3-} ions, differing in the degree of distortion. Such a structure is certainly well ordered, as already stated by Guillemin (1956). Also in the region of ν_4 vibrations, the broad absorption splits into several distinct

bands, confirming the above conclusions. The sharp 780 cm^{-1} band can correspond to the forbidden ν_1 symmetrical stretch. A rearrangement of small bands between 1000 and 1200 cm^{-1} after heating of tyrolite is visible.

The infrared spectrum of **brochantite** (Fig. 11) is similar to that recorded by Moenke (1962). In the wave-number region 1100—1150 cm^{-1} poorly resolved ν_3 bands occur which, together with a sharp ν_1 band (990 cm^{-1}), are consistent with the low sulphate site symmetry (C_1) presumed by Ross (1974). According to this author, several bands in the 700—900 cm^{-1} region are to be attributed to OH bending modes. In the lower wave-number region, ν_4 and ν_2 sulphate bands occur. They are, however, more difficult to identify. Two sharp bands at 3570 and 3590 cm^{-1}, as well as strong, poorly resolved bands at 3390—3410 cm^{-1} and a weaker one at 3280 cm^{-1}, point to the different lengths of hydrogen bonds in which participate OH groups and perhaps also H_2O molecules.

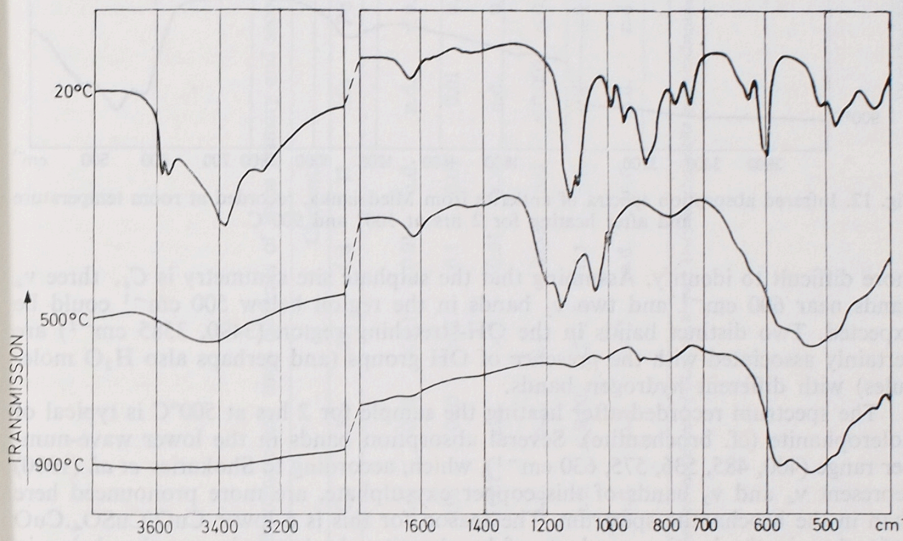

Fig. 11. Infrared absorption spectra of brochantite from Miedzianka, recorded at room temperature and after heating for 2 hrs at 500° and 900°C

The spectrum recorded after heating the sample for 2 hrs at 500°C is typical of dolerophanite $CuSO_4.CuO$ (Omori, Kerr 1963; Shokariev *et al.* 1970). Three well-resolved ν_3 bands (1040, 1155, 1205 cm^{-1}) and a sharp ν_1 band (1002 cm^{-1}) are characteristic of this sulphate, and so is the series of less sharp bands (ν_4 and ν_2) in the lower wave-number range. However, in the latter region, the superposition of tenorite bands must be taken into account. OH bands disappear.

After heating the sample for 2 hrs at 900°C, the sulphate bands disappear, several bands visible in the wave-number range 400—600 cm^{-1} being certainly mostly due to tenorite (Nyquist, Kagel 1971). The identification of this copper oxide was also performed by X-ray powder method (the strongest reflections: 2.527 — 10, 2.316 — —10, 1.866—5).

Infrared spectrum of **antlerite** (Fig. 12) is consistent with that recorded by Moenke (1962). Three well resolved ν_3 bands (1075, 1115, 1160 cm^{-1}) and a sharp ν_1 band (990 cm^{-1}) point to low sulphate site symmetry, presumably C_s (Adler, Kerr 1965; Ross 1974). Several bands in the 700—900 cm^{-1} region may be due to OH bending modes (Ross 1974). Absorption bands in the 400—700 cm^{-1} region are

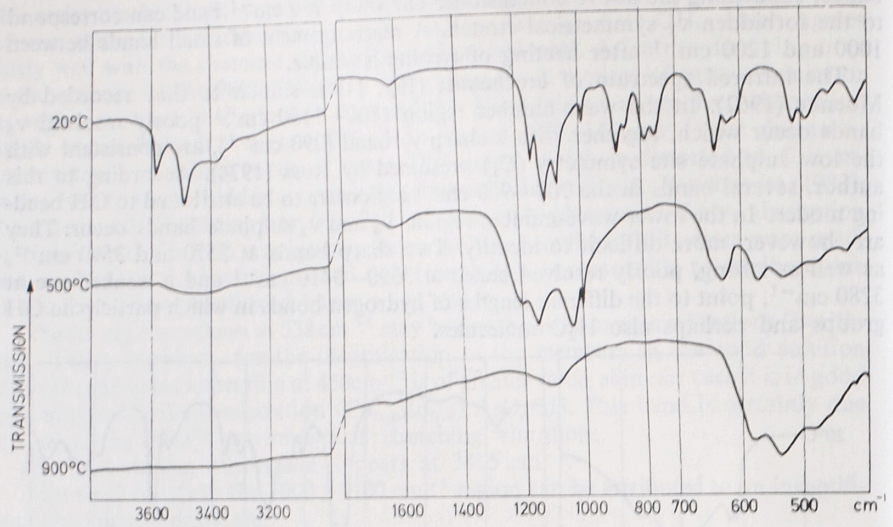

Fig. 12. Infrared absorption spectra of antlerite from Miedzianka, recorded at room temperature and after heating for 2 hrs at 500° and 900°C

more difficult to identify. Assuming that the sulphate site symmetry is C_s, three ν_4 bands near 600 cm^{-1} and two ν_2 bands in the region below 500 cm^{-1} could be expected. Two distinct bands in the OH-stretching region (3490, 3585 cm^{-1}) are certainly associated with the presence of OH groups (and perhaps also H_2O molecules) with different hydrogen bands.

The spectrum recorded after heating the sample for 2 hrs at 500°C is typical of dolerophanite (cf. brochantite). Several absorption bands in the lower wave-number range (400, 485, 536, 575, 630 cm^{-1}), which, according to Shokariev *et al.* (1970) represent ν_4 and ν_2 bands of this copper oxysulphate, are more pronounced here than in the brochantite spectrum. The reason for this is a lower $CuO/CuSO_4.CuO$ ratio than in the heating products of brochantite, the bands in question being in a lesser degree covered by tenorite absorptions.

After heating the sample for 2 hrs at 900°C, sulphate bands disappear, and several copper oxide (tenorite) absorptions are visible in the wave-number range 400—600 cm^{-1}. A weak, broad band which appears near 1100 cm^{-1} is certainly due to a small admixture of amorphous silica.

Emission spectral analysis

Subordinate and trace elements in the investigated minerals from the Miedzianka deposit were determined by semiquantitative emission spectroscopy (Tab. 5). The presence of considerable amounts of Zn in Zn-olivenite and, to a lesser degree, in the other secondary minerals is associated with Zn-bearing tennantite, an important primary mineral. Taking into account the small arsenium content in brochantite and antlerite, the substitution of zinc for copper is probable. The low iron content in all the secondary minerals points to the absence of chalcopyrite as a source mineral. The enrichment in some elements, such as Ag, Bi, Pb, Cd, may be mainly due to the decomposition of tennantite.

Table 5

Semiquantitative emission spectral analyses of subordinate and trace elements of some primary and secondary minerals from Miedzianka

Minerals	Elements												
	Fe	Mn	Co	Ni	Zn	Cd	Tl	Mo	Pb	Bi	Sb	As	Ag
Chalcocite	0.01–0.5	0.001	n.d.	0.01	⩽0.1	⩽0.01	n.d.	n.d.	⩽0.3	⩽0.01	n.d.	⩽0.1	⩽0.02
Tennantite	0.05	0.002	0.01	0.05	> 2	0.1	0.01	0.01	0.5	0.1	n.d.	> 10	0.02
Zn-olivenite	0.001	0.05	0.001	n.d.	> 2	0.01	n.d.	n.d.	0.01	0.001	n.d.	> 10	0.005
Tyrolite	0.001	⩽0.01	n.d.	n.d.	0.1	0.005	n.d.	⩽0.005	⩽0.1	⩽0.01	⩾0.001	> 10	⩽0.01
Brochantite	0.01–0.1	⩽0.001	n.d.	⩽0.002	0.2–1.5	0.1	n.d.	n.d.	⩽0.1	⩽0.01	⩽0.05	⩽0.01	⩾0.001
Antlerite	0.01	0.001	n.d.	n.d.	< 2	n.d.	n.d.	n.d.	n.d.	n.d.	n.d.	0.3	n.d.

Remark: other elements, like: Ge, Ga, In, Te, Cr, V, Sn, were examined but not detected (n.d., see above). Data for chalcocite and brochantite are based on triple analyses, those for tyrolite on double ones.

Acknowledgments. We wish to thank Dr. T. Hanczke for supplying us with fine specimens of tyrolite from Miedzianka. We are indebted to Assistant Professor Z. Rubinowski for kindly assisting in collecting of mineral samples. Prof. W. Parachoniak is thanked for recording thermograms on the "Derivatograph" apparatus.

REFERENCES

ADLER H. H., KERR P. F., 1965: Variations in infrared spectra, molecular symmetry and site symmetry of sulfate minerals. *Amer. Miner.* 50, 132—147.

BERRY L. G., 1948: Tyrolite, higginsite and cornwallite. *Amer. Miner.* 33, 3—4, 193.

BERRY L. G., 1951: Observations on conichalcite, cornwallite, euchroite, liroconite and olivenite. *Amer. Miner.* 36, 5—6, 484—503.

BRAITHWAITE R. S.W., 1983: Infrared spectroscopic analysis of the olivenite-adamite series, and of phosphate substitution in olivenite. *Miner. Mag.* 47, 51—57.

CZARNOCKI J., 1929: O tektonice okolic Miedzianki w związku ze złożami miedzi tegoż obszaru. *Pos. Nauk. Państw. Inst. Geol.* 24, 29—32.

DANA J. D., DANA E. S., PALACHE Ch., BERMAN H., FRONDELL C., 1951: The system of mineralogy. Vol. II. J. Wiley and Sons. New York—London.

[DUNIN-BARKOVSKAYA E. A.] ДУНИН-ЪАРКОВСКАЯ Э. А., 1960: О новых членах изоморфного ряда оливенит-адамин. *Зап. Всес. Мин. Общ.* 89, 4, 400—414.

[DUNIN-BARKOVSKAYA E. A.] ДУНИН-БАРКОВСКАЯ Э. А., 1962: Конихальцит и еташицит из Латчин-Ханы. *Зап. Всес. Мин. Общ.* 92, 2, 146—157.

GUILLEMIN C., 1956: Contribution à la minéralogie des arséniates, phosphates et vanadates de cuivre. I. Arséniates de cuivre. *Bull. Soc. Franc. Min. Crist.* 79, 1—3, 7—95.

JARREL O. W., 1939: Marshite and other minerals from Chuquicamata, Chile. *Amer. Miner.* 24, 10, 629—635.

LARSEN E. S., 1921: The microscopic determination of nonopaque minerals. *U. S. Geol. Survey Bull.* 679.

MINČEVA-STEFANOVA J., 1964: Zink-Olivenit aus der Lagerstätte Zapačica und über den Chemismus und die Ablagerung der Kupferarsenate. *Chemie der Erde* 23, 4, 248—258.

MOENKE H., 1962: Mineralspektren. Berlin.

MOROZEWICZ J. 1919: Staszycyt — nowy minerał złoża kruszcowego na Miedziance. *Rozpr. Wydz. Mat.-Przyr. Akad. Um.*, ser. III, 18, dz. A, 123—134.

MOROZEWICZ J., 1923: O miedziankicie. *Spr. Państw. Inst. Geol.* 24, 29—32.

MROSE M. E., 1948: Adamite from Ojuela Mine, Mexico. *Amer. Miner.* 33, 7—8, 449—457.

MROSE M. E., 1961: Vernadskite discredited: pseudomorphs of antlerite after dolerophanite. *Amer. Miner.* 46, 1—2, 146—154.

NYQUIST R. A., KAGEL R. O., 1971: Infrared spectra of inorganic compounds (3800—45 cm^{-1}). Academic Press. New York—London.

OMORI K., KERR P. F., 1963: IR studies of saline sulphate minerals. *Bull. Geol. Soc. Am.* 74, 709—734.

[ROZINOVA Je. L., MURATOV I. G.] РОЗИНОВА Е. Л., МУРАТОВ И, Г., 1973: Термоаналитическая характеристика брошантита. *Зап. Всес. Мин. Общ.* 102, 2, 217—222.

ROSS S. D., 1974: Phosphates and other oxy-anions of group V. In: The infrared spectra of minerals. Ed. V. C. Farmer. Mineralogical Society. London.

RUBINOWSKI Z., 1955: Nowe obserwacje okruszcowania na Miedziance Świętokrzyskiej. *Prz. Geol.* 6, 299—301.

RUBINOWSKI Z., 1971: Rudy metali nieżelaznych w Górach Świętokrzyskich i ich pozycja metalogeniczna. *Biul. IG* 247, 1—166.

SAPOUNTZIS E., 1972: Brochantite from Karya, Mt. Olympus (Central Greece). *N. Jb. Miner.* Monatsh. 7, 320—324.

[SHOKARIEV M. M. *et al.*] ШОКАРЕВ М. М., ВЕРШИНИНА Ф, И,, МАРГУЛИС Е. В.,1970: Инфракрасные спектры нормальных сульфатов и оксосульфатов меди, цинка, кадмия и ртути. *Шурнал Структ. Химии* 11, 151—154.

STRUNZ H., 1939: Mineralien der Descloizitgruppe. Konichalcit, Staszicit, Austinit, Duftit, Arãoxen, Volborthit, Pyrobelonit. *Ztschr. Krist.* 101, 496—506.

WOJCIECHOWSKI J., 1958: Minerały Miedzianki pod Chęcinami (Pierwsze minerały niklu na Miedziance). *Prace Muzeum Ziemi* 1, 133—152.

Tadeusz WIESER, Witold ŻABIŃSKI

ARSENIANY I SIARCZANY MIEDZI Z MIEDZIANKI KOŁO KIELC (POLSKA)

Streszczenie

Lista minerałów wtórnych ze złoża miedzi w Miedziance koło Kielc obejmuje, prócz pospolitych i dobrze znanych węglanów — malachitu i azurytu, także arseniany — Zn-oliwenit i tyrolit oraz siarczany — brochantyt i antleryt. Problem staszicytu, opisanego z tego złoża przez Morozewicza (1919) jako nowy minerał arsenianowy, pozostaje nadal kontrowersyjny: według Strunza (1939) jest to konichalcyt, zaś Guillemin (1956) i Dunin-Barkowskaja (1962) uważają go za Zn-oliwenit.

Zn-oliwenit występuje w Miedziance w dwóch odmianach, różniących się zawartością cynku (odmiana uboższa w cynk nazywana bywa *leukochalcytem*). Są one łatwe do rozpoznania m.in. metodami optycznymi. Widmo absorpcyjne w podczerwieni zarejestrowane dla Zn-oliwenitu jest typowe dla ogniwa szeregu izomorficznego oliwenit-adamin zawierającego około 40% członu adaminowego.

Tyrolit, odznaczający się często efektownym koncentryczno-promienistym wykształceniem, wykazuje różny stopień dehydratacji. Przejawia się to w pewnej zmienności współczynników załamania światła oraz odległości płaszczyzn sieciowych mierzonych na różnych jego okazach. Widmo absorpcyjne zarejestrowane po wygrzaniu próbki tyrolitu przez 2 godz. w 600°C wskazuje na porządkowanie się struktury minerału po utracie większej części wody.

Obydwa minerały arsenianowe związane są z występowaniem w złożu Zn-tennantytu (miedziankitu według Morozewicza 1923), który był minerałem pierwotnym.

Antleryt, mniej pospolity w złożu od **brochantytu**, wytrącał się z bardziej kwaśnych roztworów jako ostatni w sukcesji wtórnych minerałów miedzi, pochodzących z utlenienia β-chalkozynu. Produkty rozkładu termicznego brochantytu i antlerytu są identyczne (dolerofanit, tenoryt) i, jak można wnioskować na podstawie krzywych DTA, ich temperatury powstawania różnią się tylko nieznacznie między sobą.

OBJAŚNIENIA FIGUR

Fig. 1. Zmienność współczynników załamania światła w szeregu izomorficznym adamin-oliwenit
Fig. 2. Zmienność wartości Δd_{131}—d_{311} w szeregu izomorficznym adamin-oliwenit
Fig. 3. Dyfraktogramy rentgenowskie oliwenitu cynkowego, tyrolitu, brochantytu i antlerytu z Miedzianki, Polska
A — antleryt, *O* — oliwenit cynkowy (jako domieszki). Dyfraktometr rentgenowski Iris-5.
Fig. 4. Termogramy oliwenitu cynkowego z Miedzianki. Derywatograf
Fig. 5. Termogramy tyrolitu z Miedzianki. Termoanalizator TA-2 Mettler
Fig. 6. Termogramy tyrolitu z Miedzianki. Derywatograf
Fig. 7. Termogramy brochantytu z Miedzianki. Derywatograf
Fig. 8. Termogramy antlerytu z Miedzianki. Derywatograf
Fig. 9. Widma absorpcyjne w podczerwieni oliwenitu cynkowego z Miedzianki, zarejestrowane w temperaturze pokojowej i po wygrzaniu próbki przez 2 godz. w 700°C
Fig. 10. Widma absorpcyjne w podczerwieni tyrolitu z Miedzianki, zarejestrowane w temperaturze pokojowej i po wygrzaniu próbki przez 2 godz. w 200, 400, 600 i 800°C
Fig. 11. Widma absorpcyjne w podczerwieni brochantytu z Miedzianki zarejestrowane w temperaturze pokojowej i po wygrzaniu próbki przez 2 godz. w 500 i 900°C
Fig. 12. Widma absorpcyjne w podczerwieni antlerytu z Miedzianki zarejestrowane w temperaturze pokojowej i po wygrzaniu próbki przez 2 godz. w 500 i 900°C

OBJAŚNIENIA FOTOGRAFII

Plansza I

Fot. 1. Izometrycznie-ziarnista odmiana (druga generacja) oliwenitu cynkowego. Próbka nr 8 z Miedzianki, pow. 16×
Fot. 2. Pilśniowy agregat, złożony z włóknistego, prawie bezbarwnego oliwenitu cynkowego (tzw. leukochalcytu) trzeciej generacji. Widoczny w lewej części razem z azurytem (ciemne pole) i kalcytem (białe pole). Próbka nr 1460, pow. 17×
Fot. 3. Półkuliste, promienisto-włókniste agregaty tyrolitu. Próbka nr 76, pow. 16×
Fot. 4. Promieniście ułożone włókna tyrolitu z częściowo odwodnionym rąbkiem (jaśniejszy pas). Próbka nr 1, pow. 8×

Plansza II

Fot. 5. Inny obraz próbki tyrolitu nr 1 (p. fot. 4), pow. 4×
Fot. 6. Grupy kryształów brochantytu (ciemne pola z jasnymi punktami=lśniącymi ściankami, np. środkowa górna część). Próbka nr 1470, pow. 16×
Fot. 7. Proszkowe agregaty antlerytu (jasnoszare obszary w części środkowej). Próbka nr 112, pow. 16×

Tadeusz WIZER, Witold ŻABIŃSKI

ARSENATY I SUŁFATY MIEDZI Z MIEDZIANKI KOŁO KIELC (POLSKA)

Резюме

Перечень вторичных минералов из медного месторождения Медзянка около Кельц, кроме обычных и хорошо известных карбонатов — малахита и азурита, включает также арсенаты — Zn-оливенит и тиролит, а также сульфаты — брошантит и антлерит. Проблема сташицита, описанного в этом месторождении Морозевичем (1919) как новый арсенатный минерал, все оспаривается: по Штрунцу (1939) он является конихальцитом, Гильемен (1956) и Дунин-Барковская (1962) считают, что он представляет собой Zn-оливенит.

Zn-оливенит присутствует в Медзянке в двух разновидностях, отличающихся содержанием цинка (разновидность беднее цинком называют лейкохальцитом). Они легко различаются, в частности оптическими методами. ИК-спектр поглощения Zn-оливенита типичен для члена изоморфного ряда оливенит-адамин, содержащего около 40% адаминового члена.

Тиролит, характеризующийся часто эффектным радиально-концентрическим строением, обнаруживает различную степень дегидратации. Это проявляется в некоторой изменчивости показателей преломления, а также межплоскостных расстояний решетки, измеряемых на разных его образцах. Спектр поглощения, зафиксированный после прогрева образца тиролита в течение 2 часов в температуре 600°C, указывает на упорядочивание структуры минерала после потери большинства воды.

Оба арсенатные минералы связаны с присутствием в месторождении Zn-теннантита (медзянкит по Морозевичу, 1923), который являлся первичным минералом.

Антлерит, менее распространенный в месторождении чем брошантит, выпадал из более кислых растворов как последний в сукцессии вторичных медных минералов, происходящих из окисления ß-халькозина. Продукты

термического разложения брошантита и антлерита идентичны (долерофанит, тенорит), и, как можно полагать на основании кривых ДТА, температуры их образования лишь незначительно расходятся между собой.

ОБЪЯСНЕНИЯ К ФИГУРАМ

Фиг. 1. Изменчивость коэффициентов преломления света в изоморфном ряду адамин-оливенит
Фиг. 2. Изменчивость значений Δd_{131}—d_{311} в изоморном ряду адамин-оливенит
Фиг. 3. Рентгеновские дифрактограммы цинкового оливенита, тиролита, брошантита и антлерита из Медзянки, Польша. Рентгеновский дифрактометр Iris-5
A — антлерит, *O* — цинковый оливенит (как примесь)
Фиг. 4. Термограммы цинкового оливенита из Медзянки. Дериватограф
Фиг. 5. Термограммы тиролита из Медзянки. Термоанализатор TA-2 Mettler
Фиг. 6. Термограммы тиролита из Медзянки. Дериватограф
Фиг. 7. Термограммы брошантита из Медзянки. Дериватограф
Фиг. 8. Термограммы антлерита из Медзянки. Дериватограф
Фиг. 9. ИК-спектры поглощения цинкового оливенита из Медзянки, зафиксированные в комнатной температуре и после прогревания образца в температуре 700°C в течение 2-х часов
Фиг. 10. ИК-спектры поглощения тиролита из Медзянки, зафиксированные в комнатной температуре и после прогревания образца в температурах 200, 400, 600 и 800°C в течение 2-х часов
Фиг. 11. ИК-спектры поглощения брошантита из Медзянки, зафиксированные в комнатной температуре и после прогревания образца в температурах 500 и 900°C в течение 2-х часов
Фиг. 12. ИК-спектры поглощения антлерита из Медзянки, зафиксированные в комнатной температуре и после прогревания образца в температурах 500 и 900°C в течение 2-х часов

ОБЪЯСНЕНИЯ К ФОТОГРАФИЯМ

Таблица I

Фото 1. Изометрически-зернистая разновидность цинкового оливенита (вторая генерация). Медзянка. Образец № 8. Увел. 16×
Фото 2. Войлочный агрегат, сложенный волокнистым почти бесцветным цинковым оливенитом третьей генерации (так незываемым лейкохальцитом). Он заметен в левой части вместе с азуритом (темное поле) и кальцитом (светлое поле). Образец № 1460. Увел. 17×
Фото 3. Полусферические радиально-волокнистые агрегаты тиролита. Образец № 76. Увел. 16×
Фото 4. Радиально расположенные волокна тиролита с частично обезвоженной каемкой (более светлая полоса). Образец № 1. Увел. 8×

Таблица II

Фото 5. Другое изображение образца тиролита № 1 (см. фото 4). Увел. 4×
Фото 6. Группы кристаллов брошантита (темные участки со светлыми точками=блестящими гранями, например в середине верхней части). Образец № 1470. Увел. 16×
Фото 7. Порошковые агрегаты антлерита (светло-серые участки в средней части). Образец № 112. Увел. 16×

EXPLANATIONS OF PLATES

Plate I

Phot. 1. Isometric-granular variety (second generation) of zincian olivenite. Sample no 8 from Miedzianka, magn. 16×

Phot. 2. Felt-like aggregate, composed of fibrous, almost colourless zincian olivenite (so-called leucochalcite) of third generation. Visible in the left part with azurite (dark area) and calcite (white area). Sample no. 1460, magn. 17×

Phot. 3. Hemispherical, fibrous-radial aggregates of tyrolite. Sample no 76, magn. 16×

Phot. 4. Radiating fibers of tyrolite with partly dehydrated rim (lighter zone). Sample no 1, magn. 8×

Plate II

Phot. 5. Another view of tyrolite sample no 1 (see Phot. 4), magn. 4×

Phot. 6. Brochantite crystal groups (dark areas with light points = shining facelets, e. g. middle upper part). Sample no 1470, magn. 16×

Phot. 7. Antlerite powdery aggregates (light grey areas in middle part). Sample no 112, magn. 16×

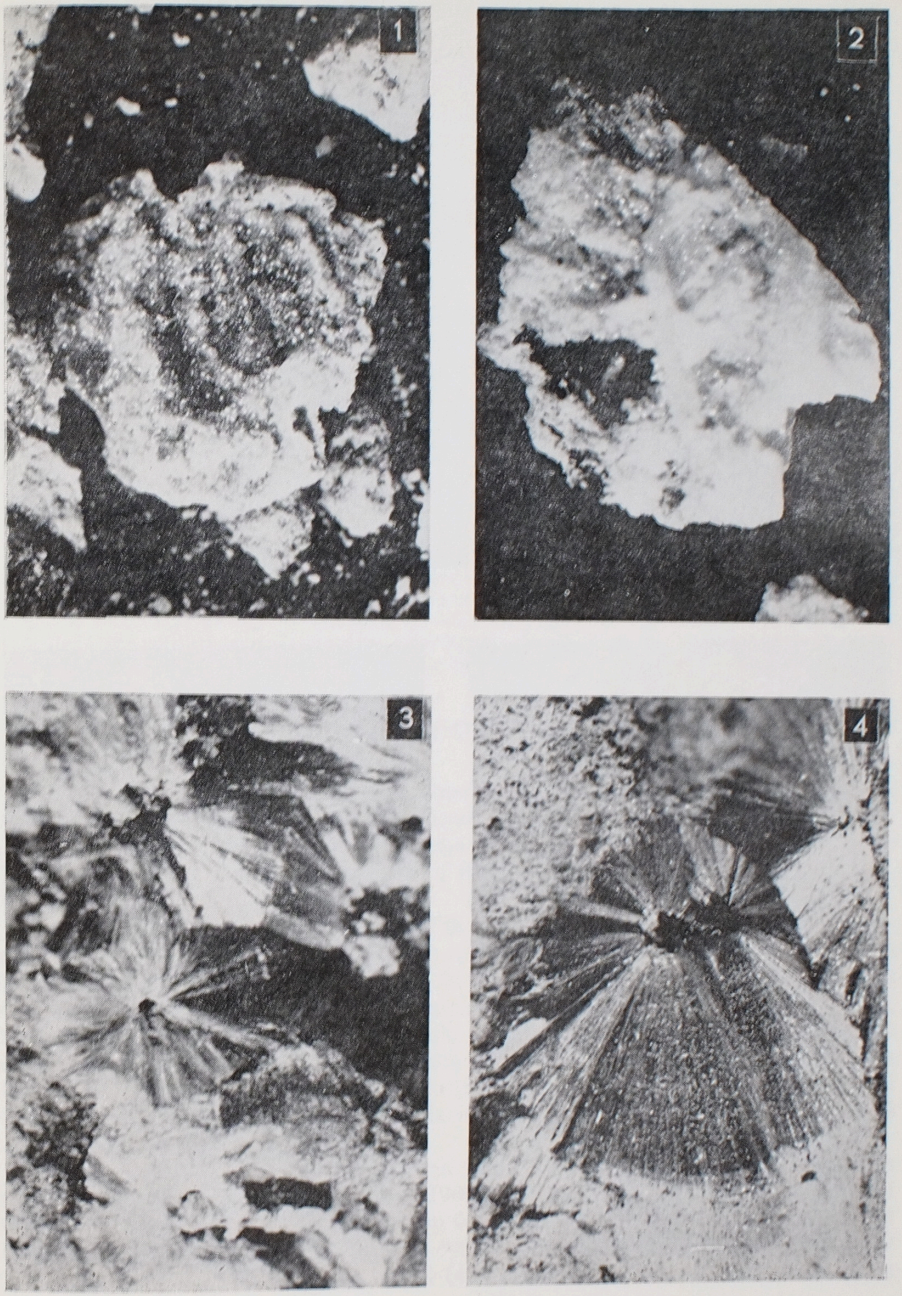

Tadeusz Wieser, Witold Żabiński — Copper arsenate and sulphate minerals from Miedzianka near Kielce (Poland)

Tadeusz Wieser, Witold Żabiński — Copper arsenate and sulphate minerals from Miedzianka near Kielce (Poland)